Radical Anion Yield, Stability and Electrical Conductivity of Naphthalene Diimide Copolymers *n*-Doped with Tertiary Amines

*Simon B. Schmidt,[§] Markus Hönig,[§] Younghun Shin,[§] Marco Cassinelli,[#] Andrea Perinot,[#] Mario Caironi,[#] Xuechen Jiao,[+] Christopher R. McNeill,[+] Daniele Fazzi,[‡] Till Biskup[&] and Michael Sommer[§]**

[§]Polymer Chemistry, Institute for Chemistry, Chemnitz University of Technology, Straße der Nationen 62, 09111 Chemnitz, Germany

[#]Center for Nano Science and Technology @PoliMi, Istituto Italiano di Tecnologia, Via Pascoli, 70/3, 20133 Milano, Italy

[+]Department of Materials Science and Engineering, Monash University, Wellington Road, Clayton, Victoria 3800, Australia

[‡]Institut fu□r Physikalische Chemie, Department Chemie, Universita□t zu Ko□ln, Luxemburger Str. 116, 50939 Ko□ln, Germany

[&]Institut für Physikalische Chemie, Albert-Ludwigs-Universität Freiburg, Albertstraße 21, 79104 Freiburg, Germany†

KEYWORDS: Naphthalene diimide (NDI), n-type copolymers, self-doping, radical anion, air stability, tertiary amine, electron transfer, torsion angles

ABSTRACT

Doped organic semiconductors are required for applications such as organic solar cells, organic light-emitting diodes and thermoelectric generators. To further establish structure-property relationships and improve the efficiency of these devices, electron acceptor conjugated polymers and suitable doping schemes are required. A key criterion is a sufficiently low lowest unoccupied molecular orbital (LUMO), which enables air-stability of excess electrons. In this work, a series of naphthalene diimide (NDI) copolymers with varying highest occupied molecular orbital (HOMO) and LUMO energy levels are made and used to investigate photochemically and thermally induced electron transfer from a small molecule NDI carrying dimethylaminopropyl (DMAP) side chains. Density functional theory calculations, UV-vis and electron spin resonance (ESR) spectroscopies indicate that the LUMO energy level of the NDI copolymer governs thermal electron transfer from the HOMO of the DMAP side chain and dictates air stability of the corresponding radical anions. Conversely, photoinduced electron transfer from DMAP to the NDI copolymer is governed by the position of the HOMO energy levels. While dicyano-substituted NDI copolymers with very low LUMO levels display the highest radical anion yield and excellent air stability, their conductivity is limited by electron mobility, which in turn is strongly influenced by backbone torsion and localized radical anions. These results establish fundamental structure-function relationships and shine light on the use of simple and cost-economic, covalently bound tertiary amines as potential n-dopants for electron acceptor copolymers.

1. Introduction

Electronic structure, doping processes, electronic conductivity and air stability of electron acceptor conjugated materials and polymers in particular, are crucial for the further development of efficient electronic devices such as organic photovoltaics, light emitting diodes, or thermoelectric generators.[1-3] These properties heavily depend, among other parameters, on their frontier orbital energy levels.[4–7] To increase charge carrier densities and thus electrical conductivity of electron acceptor polymers, n-doping is necessary.[8,9] Unlike inorganic semiconductors, doping of organic semiconductors refers to a redox process, in which electron acceptor and donor materials are chemically reduced and oxidized, respectively, on a sub-stochiometric level.[10] To obtain a reasonable n-doping efficacy, the material's electron affinity must be more negative than the ionization potential of the dopant used.[11,12] It is generally assumed that air-stability of the resulting radical anions requires a lowest unoccupied molecular orbital (LUMO) more negative than -4.0 eV.[13–15] A class of air stable materials with excellent electron transport properties is built from substituted benzodifurandione- phenylenevinylene derivatives.[4,16] Also naphthalene diimide (NDI)-based materials are popular candidates for n-type semiconductors and were used in several forms, ranging from small molecules,[17–20] supramolecular assemblies,[21,22] side-chain polymers[23] to conjugated main chain copolymers.[24,25] PNDIT2, also referred to as N2200, is a conjugated donor-acceptor copolymer composed of alternating units of NDI and bithiophene (T2), which has been n-doped with dihydro-1H-benzimidazole-2-yl (N-DBI) derivatives,[26] amines,[27,28] anions[29] as well as metallocenes.[30,31] The doping efficacy of PNDIT2 with benzimidazoles, however, is limited by their miscibility.[32] This is an often seen limitation especially for semicrystalline copolymers, as for the doping of organic semiconductors a significant amount of dopant is needed (typically 5-30 wt%).[33] Attempts have been made to increase miscibility of PNDIT2 with benzimidazoles by either restricting the degree of crystallinity and/or optimizing the structure of the dopant or using polar side chains.[26,34,35] Alternatively, the issue of the dopant phase separation can be addressed by an intrinsic doping or self-doping strategy.[36–38] In this case, the chemical functionality responsible for doping, which may be a tertiary amine or quaternary ammonium group, is covalently linked to the conjugated polymer backbone.[38–41] While the mechanism involves doping via electron transfer from the amine to the electron acceptor,[40,42–44] in case of quaternary ammonium-containing side chains details of this mechanism may differ.[12,38–40,43,45,46] Next to these

mechanistic studies, such doping processes are often correlated with device characteristics such as electrical conductivity for a given system,[41] but structure-function relationships are more often reported for transistor applications.[47–49]

Previously, we have used binary blends of small molecule NDI derivatives as a model system to study electron transfer from dimethylaminopropyl (DMAP) side chains attached to NDI to a second NDI derivative of varying energy level. By introducing aromatic core substituents of different electron withdrawing or donating strength, we investigated radical anion yield as well as air stability, and also found that DMAP-NDI forms molecularly mixed morphologies with NDI derivatives.[15]

In this work, a series of naphthalene diimide (NDI) copolymers with varying highest occupied molecular orbital (HOMO) and LUMO are employed to investigate photochemically and thermally induced electron transfer from a small molecule NDI carrying DMAP side chains. By using optical, thermal, electronic and magnetic measurements, as well as computational chemistry, correlations between energy levels, doping efficacy, air stability of radical anions, morphology, backbone torsion and electrical conductivity are investigated.

2. Results and Discussion

In this study, five different NDI copolymers were obtained from the combination of either unsubstituted NDI or dicyanated NDI ($NDICN_2$) as acceptor monomer, and phenylene (P), bithophene (T2) or 2,2´-bithiazole (BTz) as donor comonomer. The synthesis of the resulting copolymers PNDIT2, PNDIP, PNDIBTz, $PNDICN_2T2$, and $PNDICN_2P$ was carried out using either direct arylation polycondensation (DAP), Suzuki polycondensation (SPC) or Stille polycondensation (SP), as described in the Supporting Information. For doping experiments, DMAP-NDI was used for all copolymers. Chart 1 shows the chemical structures of all the copolymers, Table 1 summarizes the molecular characterization and their optoelectronic properties.

Chart 1. Structures of the studied NDI copolymers and DMAP-NDI.

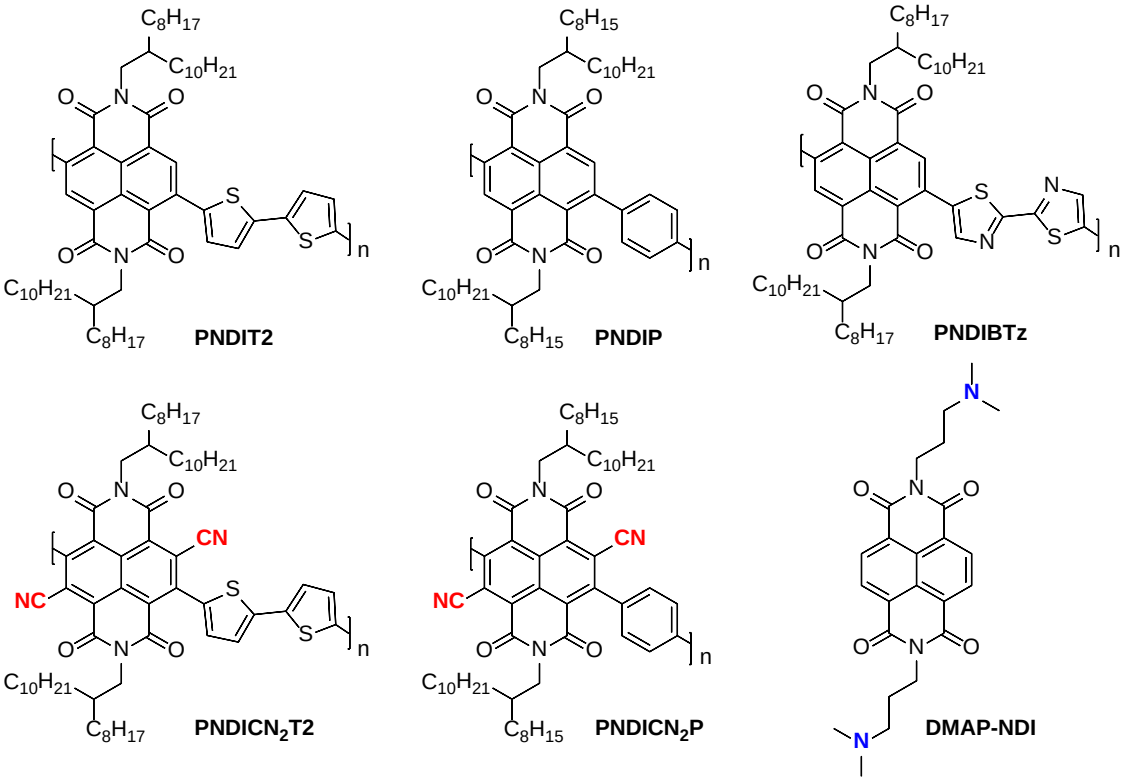

Table 1. Molecular weights, energy levels and optical band gaps of the NDI copolymers in film compared to DMAP-NDI, all mass and energy values are given in [kg·mol^{-1}] and [eV], respectively.

compound	M_n (SEC)	M_w (SEC)	LUMO (CV)	LUMO (theo)	HOMO	HOMO (theo)	$E_{opt, exp}$	E^{vert}_{S0-S1}	dihedral angle α
DMAP-NDI			-3.90[b]15	-3.59	-5.05[a]15 -6.84[b]15	-5.82[a] -7.254[b]	2.94[b]15		
PNDIT2	66	243	-3.69	-3.48	-5.19	-5.59	1.50	2.86 (f = 0.463)	46°
PNDICN$_2$T2	32	70	-4.42	4.12	-5.92	-5.76	1.50	2.58 (f = 0.031)	63°
PNDIP	22	48	-3.81	-3.41	-6.16	-6.42	2.36	3.42 (f = 0.188)	58°
PNDICN$_2$P	26	36	-4.26	4.11	-6.53	-6.73	2.27	3.16 (f = 0.005)	80°
PNDIBTz	39	99	-4.06	-3.73	-6.21	-6.17	2.15	3.26 (f = 0.155)	54°

M_n/ M_w are number / weight average molecular weights from size exclusion chromatography (SEC). $E_{opt, exp}$ and $E_{opt, theo}$ are optical band gaps from UV-Visible spectroscopy / cyclic voltammetry and density functional theory calculations, respectively. [a]values of DMAP unit [b]values of NDI core. Vertical transition energy (E^{vert}_{S0-S1}) for the S_0-S_1 transitions and associated oscillator strength (f) as computed at the TD-ω-B97X-D/6-311G* level of theory (gas phase). Molecular orbital energies (HOMO and LUMO) and dihedral angles are here reported at the B3LYP/6-311G* level (gas phase).

To vary the LUMO energy level significantly and surpass the anticipated -4.0 eV threshold required for air stability of radical anions, cyanated NDICN$_2$ was used as building block.[49,50] As comonomers, employed to further vary the HOMO energy level, T2, P and BTz, all exhibiting different donor strength, were additionally used. All cyanated NDI copolymers were prepared by Stille polycondensation; attempts to use DAP or SPC were unsuccessful. For the synthesis of literature-unknown PNDICN$_2$P, the same reaction conditions that produced high molecular weights of PNDICN$_2$T2 led to oligomers only. Optimizing these conditions by changing ligand, solvent, temperature and monomer concentration improved both the yield and the molecular weight (see Table S1 in the Supporting Information). The best conditions were obtained with tri(2-furyl)phosphine as ligand in tetrahydrofuran at 80 °C, furnishing an average number of molecular weight M_n = 26 kg·mol^{-1}. Thus, this polymer, to the best of our knowledge, has been synthesized for the first time. The copolymers PNDIT2[51] and PNDIBTz[52]

were prepared by DAP, following a procedure reported elsewhere. PNDIP with M_n = 22 kg·mol^{-1} was prepared by modified SPC (see supporting information for details).[53] For NMR characterization and molecular weight determination by size exclusion chromatography see Supporting Information (Table 1, Figures S1-4).

The optoelectronic properties of the NDI copolymers were examined by both cyclic voltammetry (CV) (Figure 1) and UV-Vis spectroscopy of thin films (Figure 2).

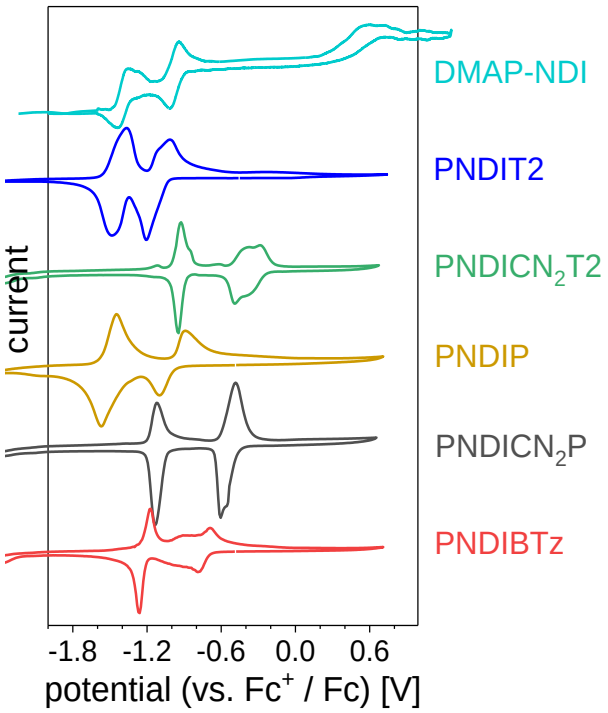

Figure 1. Cyclic voltammograms of NDI copolymer films measured in acetonitrile with NBu_4PF_6 as electrolyte under argon. Scan rate 50 mV·s^{-1}.

From the CV curves the LUMO energy levels were determined (LUMO = −4.8 eV − $E_{1/2}^{red}$). The optical bandgaps were determined from the UV-Vis measurements (Figure 2). Subtraction from the electrochemically determined LUMO gave a first estimation of the corresponding HOMO energy levels. Table 1 summarizes the frontier energy levels of all compounds.

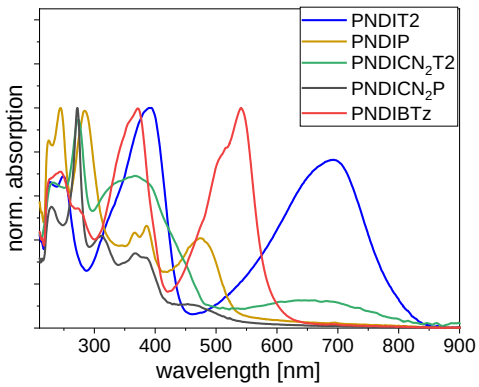

Figure 2. UV-Vis spectra of thin films spin coated from chloroform.

The optical band gaps (i.e. S0-S1 vertical transition) were calculated by time-dependent density functional theory (TD-DFT) on monomers (i.e., single repeat unit) of each compound, instead of the corresponding oligomer representative of the polymer chain. The computed values are intrinsically overestimated, nevertheless they reflect the experimental trend, showing the highest gap for the phenyl derivatives (PNDIP and PNDICN$_2$P) and the 2,2´-bithiazole species (PNDIBTz). Calculations were performed using the range-separated functional ω-B97X-D to better describe charge-transfer excitations, and the triple split valence basis set 6-311G*, on top of the respective optimized geometries for the monomers (Table 1). Another set of DFT calculations, performed at the B3LYP/6-311G* level (gas phase), was carried out to compare the computed HOMO energies to those experimentally derived. It is well known that B3LYP does not describe charge transfer (CT) excitations correctly underestimating the value,[54] however it provides a reasonable description for the molecular orbital levels. In Table 1 we compared the experimental HOMO energies with the computed one, showing reasonable correlation. All calculations were performed with Gaussian16 B.01.[55]

From Table 1, the influence of both the cyano substituents and the donor comonomers on the energy levels of the NDI copolymers is directly visible. Taking PNDIT2 as a reference, PNDIP and PNDIBTz containing the less electron rich comonomers P and BTz exhibit lowered LUMO values by about 0.1 eV and 0.4 eV, respectively. The LUMO energy levels of PNDICN$_2$T2 and PNDICN$_2$P are strongly lowered by 0.7 and 0.5 eV, respectively, resulting from the introduction of cyano substituents. These values now fall well below the threshold value of ~

−4.0 eV required for air-stable doping.[56] Together with the rather high LUMO, a HOMO energy level of -5.2 eV is determined for PNDIT2, which is just below that of the DMAP side chain. With almost 2.2 eV, the optical band gap of PNDIBTz is significantly larger and a HOMO energy level of -6.2 eV is obtained. As desired, phenylene as comonomer is a weaker electron donor and exerts a less strong charge transfer (CT) effect. Thus, the optical band gap of PNDIP is determined as 2.4 eV, 0.9 eV larger than of PNDIT2, and the HOMO energy level of about -6.2 eV is 1.0 eV lower. Compared to their non-cyanated analogues, PNDICN_2T2 and PNDICN_2P exhibit reduced charge transfer absorption bands. The reduction of the electron density at the NDI core introduced by two CN substituents should lead to increased intramolecular charge transfer for a given comonomer. The fact that the opposite case is observed indicates significant backbone torsion as a result of the increased steric demand of the CN groups (Table 1, Figure 3). Due to this increased backbone torsion, electronic interaction between donor and acceptor building blocks is limited leading to low intensity CT bands.[57–59] Due to the already low LUMO energy levels of the cyanated copolymers, HOMO energy levels of PNDICN_2T2 and PNDICN_2P are determined to be -5.9 eV and -6.5 eV, respectively, which are 0.7 and 1.3 eV lower than of PNDIT2.

The varying intensities of the charge transfer absorption bands can be explained by the varying dihedral angles between the NDI core and the comonomer as a result of sterical hindrance. These effects are also seen from DFT calculations. Figure 3 shows geometry-optimized repeat units and distribution of electron density in the LUMO of the five copolymers, were the varying dihedral angle α is seen. The values are also compiled in Table 1.

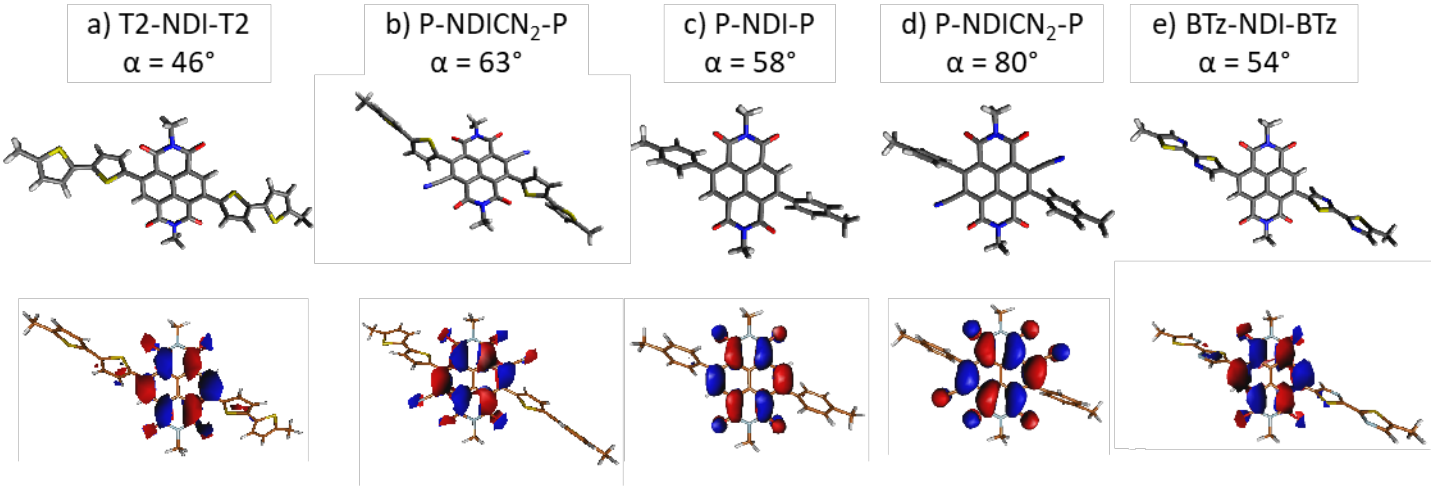

Figure 3. DFT calculations (B3LYP/6-311G*) on monomer models showing torsional angles (top) and LUMO (bottom, isosurface value 0.001Å^3) for the five different structures, namely a) T2-NDI-T2, b) T2-NDICN$_2$-T2, c) Ph-NDI-Ph, d) Ph-NDICN$_2$-Ph, e) BTz-NDI-BTz.

Thermally and photoinduced electron transfer (PET) from DMAP-NDI to the NDI copolymers were first examined by UV-Vis spectroscopy. Blend films containing 10 wt% DMAP-NDI spin coated from chloroform were irradiated with UV-light (366 nm) or annealed at 200 °C for 5 minutes under argon. The development of radical anions was followed by the relative change of the optical spectra (Figure 4). The films were then exposed to air to test the air stability of the radical anions (Figure S5 in the Supporting Information). NDI radical anions show characteristic bands at 500 nm and 780 nm,[29,60,61] marked by grey lines.

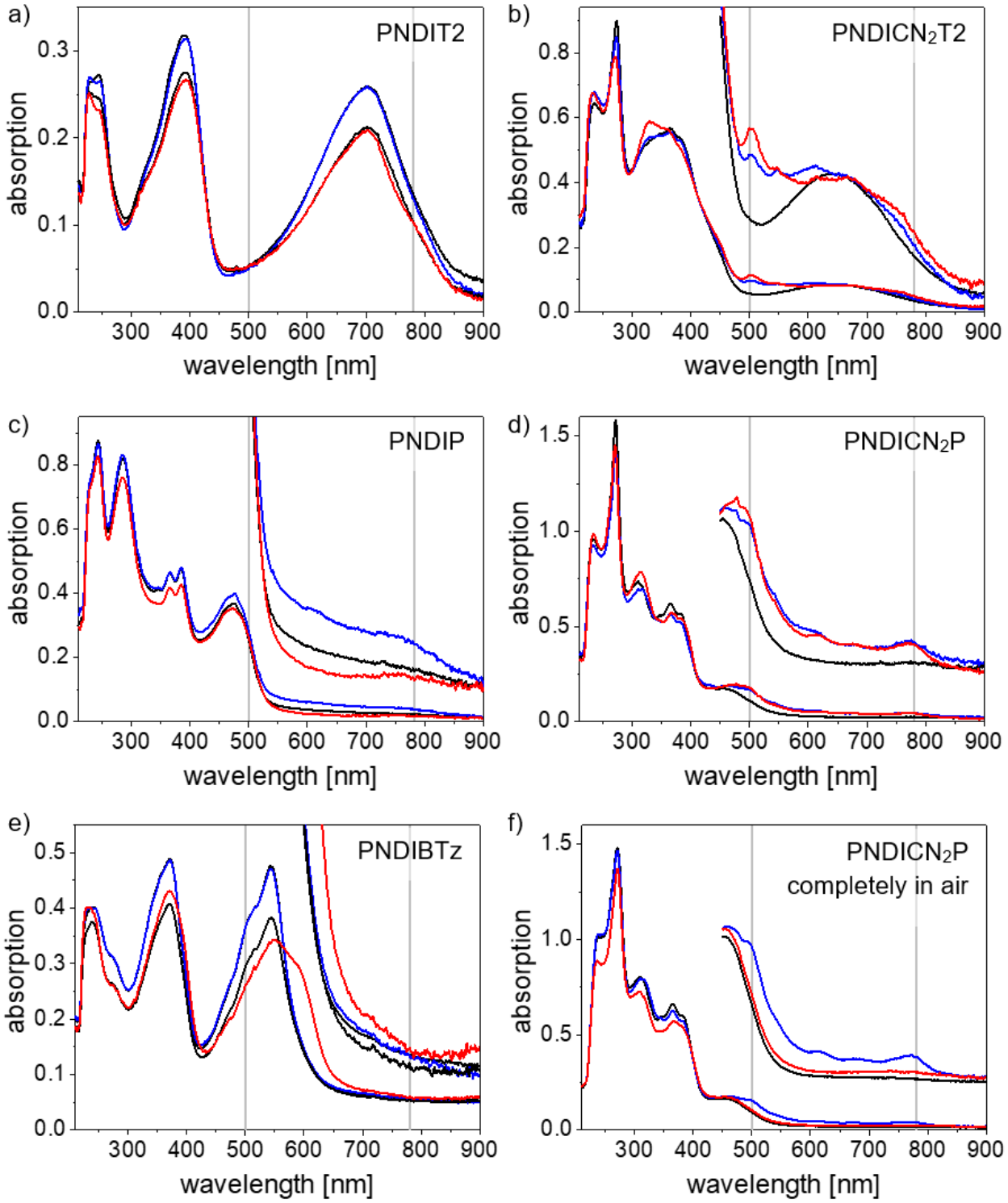

Figure 4. UV-Vis thin film absorption spectra of NDI copolymers containing 10 wt% DMAP-NDI. a) PNDIT2, b) PNDICN$_2$T2, c) PNDIP, d) PNDICN$_2$P, e) PNDIBTz and f) PNDICN$_2$P in air. Black: as prepared, blue: after 5 min UV-irradiation, red: after 5 min annealing at 200 °C. The insets show y-axes enlarged sections. The grey lines at 500 and 780 nm indicate characteristic absorption bands of NDI small molecule radical anions. a) contains two black curves as two different films were used for thermal and photochemical doping.

The absorption spectrum of PNDIT2/DMAP-NDI did not show pronounced changes after thermal or UV treatment (Figure 4a). In contrast, PNDICN_2T2 showed clear new bands at 500 and 780 nm, which are typical absorptions of radical anions of NDI small molecules[15,29,60,61] (Figure 4b). After exposure to air, the absorption spectrum of the UV-irradiated film remained almost unchanged, suggesting excellent air stability of the radical anions in both thermally and photochemically activated films (see also Figure S5 in the SI). PNDIP films also exhibited radical anion signatures (Figure 4c), but these changes of the optical spectra disappeared when exposing the films to air. Again, additional cyano groups in PNDICN_2P caused more intense radical anion bands, which remained under ambient conditions (Figure 4d). Direct irradiation of PNDICN_2P in air gave the same spectrum as compared to inert conditions (Figure 4f). Thus, this material can be processed and doped under ambient conditions, which facilitates the handling and simplifies the device preparation. PNDIBTz does neither exhibit a clear NDI radical anion peak at 780 nm after photoactivation nor after thermal treatment (Figure 4e). Thermal activation of PNDIBTz led to changes of the CT band structure, which we believe is caused by morphological changes during annealing.

Thus, all cyanated NDI copolymers show clear signs of radical anion formation, which are air stable at the same time. However, the sterical hindrance between the NDI core and the donor comonomer causes large torsional angles, visible by both weak CT bands and radical anion absorption bands, which appear similar compared to their small molecule analogs. In addition to UV-Vis absorption investigations, and to further quantify the radical anion formation, continuous wave electron paramagnetic spin resonance (cw-EPR) measurements were performed. For this purpose, films were prepared by drop casting the blend solutions onto quartz glass substrates. To enable reasonable comparison of cw-EPR data, the drop casted volume and sample area was maintained constant. Similar to UV-vis measurements, photochemical and thermal activation processes were performed under inert conditions. Cw-EPR signal intensities were recorded and compared before and after the activation, as well as after air exposure. Figure 5 gives a direct comparison of all EPR intensities obtained from the double integral of the spectra (see Figures S6, S7 for corresponding spectra and Table S2 for tabulated values).

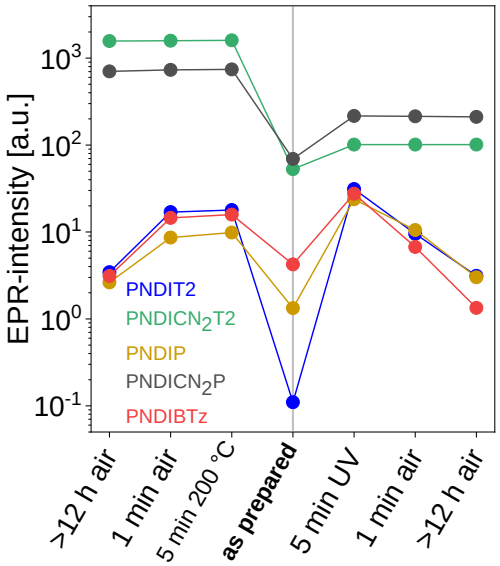

Figure 5. EPR signal intensities (determined from the cw-EPR double integral) of the NDI copolymers in films with 10 wt% DMAP-NDI directly after activation under N_2 and after air contact.

It becomes apparent that the as-prepared films of cyanated NDI copolymers already give strong EPR signals. After the activation, a further increase in EPR intensity is found compared to the corresponding copolymers without cyano groups, both for thermal as well as for the photochemical activation. Thus, thermally activated films of PNDICN_2T2 and PNDICN_2P show increased intensities by factors of 90 and 75, respectively, compared to their corresponding analog without cyano groups. All non-cyanated copolymers produce fewer radical anions and exhibit drastically lower EPR intensities than those of their cyanated analogs. Interestingly, the non-cyanated copolymers exhibit higher EPR signal intensities after UV radiation than with thermal activation. The air stability of the cyanated NDI copolymers already seen by UV-vis spectroscopy is also confirmed by EPR spectroscopy. After 12 h air exposure of all non-cyanated NDI copolymers, their EPR intensities almost vanished completely, indicating complete loss of the doping. In contrast, EPR signal intensities of doped PNDICN_2T2 and PNDICN_2P films practically do not change while exposed to air. From the determined energy levels and the trends in radical anion intensities, we propose the two simple schemes shown in Figure 6b for photochemically, and in Figure 6c for thermally activated doping, compared to the DFT calculated energy levels (Figure 6a).

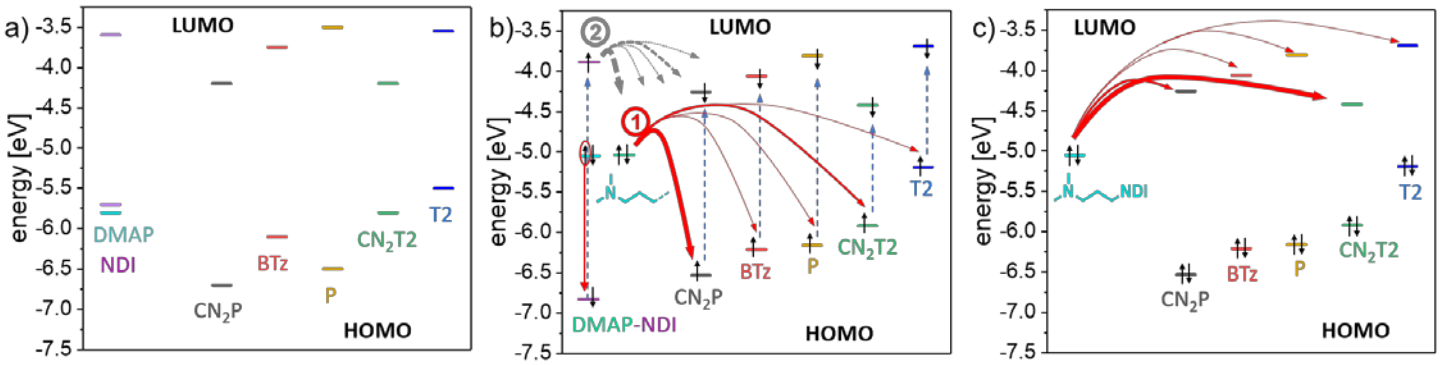

Figure 6. Schematic representation of a) computed and b,c) experimentally determined frontier energy levels with photochemically (b) and thermally induced electron transfer (c) indicated between DMAP-NDI and NDI copolymers. The red line widths correspond to qualitative trends of EPR signal intensity. In b), processes 1 and 2 depict direct electron transfer from DMAP and DMAP-NDI radical anion to copolymer, respectively.

In case of PET, the generated excitations and resulting holes in the HOMO of the copolymer are regenerated by electron transfer from the DMAP side chain, yielding a radical anion on the NDI unit and a radical cation on the nitrogen of the DMAP side chain (process 1, Figure 6b). One major parameter governing the extent of this PET is the energy offset between these HOMOs. Here, the comparison between the two cyanated copolymers PNDICN_2P and PNDICN_2T2 is instructive. PNDICN_2P with the lowest HOMO (-6.53 eV) also shows the highest doping yield, while PNDICN_2T2 exhibiting a higher HOMO (-5.92 eV) is less doped under the same conditions. The other three copolymers have varied HOMO energy levels as well, but do not follow this trend; all show rather low EPR intensities (cf Figure 5). Another process that is possible is the photo-induced generation of radical anions in DMAP-NDI first followed by electron transfer from to the copolymer chain (process 2, Figure 6b). DMAP-NDI forms radical anions upon excitation as described previously.[15] These radical anions may undergo electron transfer to nearby copolymer chains. As the excitation wavelength (365 nm) excites both DMAP-NDI as well as all copolymers, processes 1 and 2 are both possible. Their identification and contribution to the final state is, however, unclear and requires further theoretical and experimental investigations.

For thermal activation, the comparison between the two cyanated copolymers PNDICN$_2$P and PNDICN$_2$T2 depicts the effect of the LUMO energy level on radical anion yield (Figure 6c). PNDICN$_2$P and PNDICN$_2$T2 have LUMOs of -4.42 and -4.26 eV, respectively. Thus, the energy offset from DMAP to the LUMO of PNDICN$_2$T2 is smaller, hence a larger radical anion yield is found. A lower, but still considerably intense EPR signal intensity is obtained for PNDICN$_2$P, which has the second lowest LUMO. Again, the remaining three non-cyanated NDI copolymers with higher LUMOs exhibit very weak EPR signals. This simple energy diagram in Figure 6c explains the trends of radical anion intensities of the cyanated copolymers compared to the non-cyanated ones. Further details underlying this energetic uphill process with the herein determined, relatively large DMAP HOMO / NDI copolymer LUMO gap of 0.63 - 0.79 eV is subject to further investigations.

So far electronic arguments for radical anion formation were put forward. To further elucidate possible morphological factors influencing the electron transfer, we employed differential scanning calorimetry (DSC) and X-ray scattering on thin films. Figure 7 shows DSC curves of pristine PNDIT2, PNDIBTz and PNDICN$_2$T2 as well as their as prepared blends with 10 wt% DMAP-NDI (for complete thermal characterization see Figures S8-S10). Due to the limited thermal stability of DMAP-NDI, the accessible temperature range for blends was limited to 250 °C, but high enough to probe potential melting of DMAP-NDI domains segregated within the blend (T_m DMAP-NDI: 225 °C, see Figure S10). Semicrystalline PNDIT2 and PNDIBTz displayed weak endothermic signals at temperatures ~225 °C, which may be assigned to melting of DMAP-NDI. PNDIBTz did not show detectable main chain melting in accordance with the literature.[52] PNDIP/ DMAP-NDI blends did not show clear signatures of main chain melting, but eventually a weak signal of melting of DMAP-NDI domains. PNDICN$_2$T2 exhibited a different behavior. While main chain melting was absent again within the accessible temperature range, a coupled exothermic/ endothermic process was detected in the first heating trace, but no longer visible during subsequent cooling and heating cycles. Similar to cyano-substituted NDI small molecules, which also undergo thermally induced electron transfer with DMAP-NDI,[15] we hypothesize that the exothermic signal does not arise from recrystallization but from electron transfer. This process may be coupled to melting of a new mixed phase. The observation of DMAP-NDI melting in PNDIT2 and PNDIBTz blends, but not PNDICN$_2$T2 blends,

suggests enhanced molecular distribution of DMAP-NDI in the latter, and may provide an additional factor causing the high radical anion yields of the cyanated copolymers.

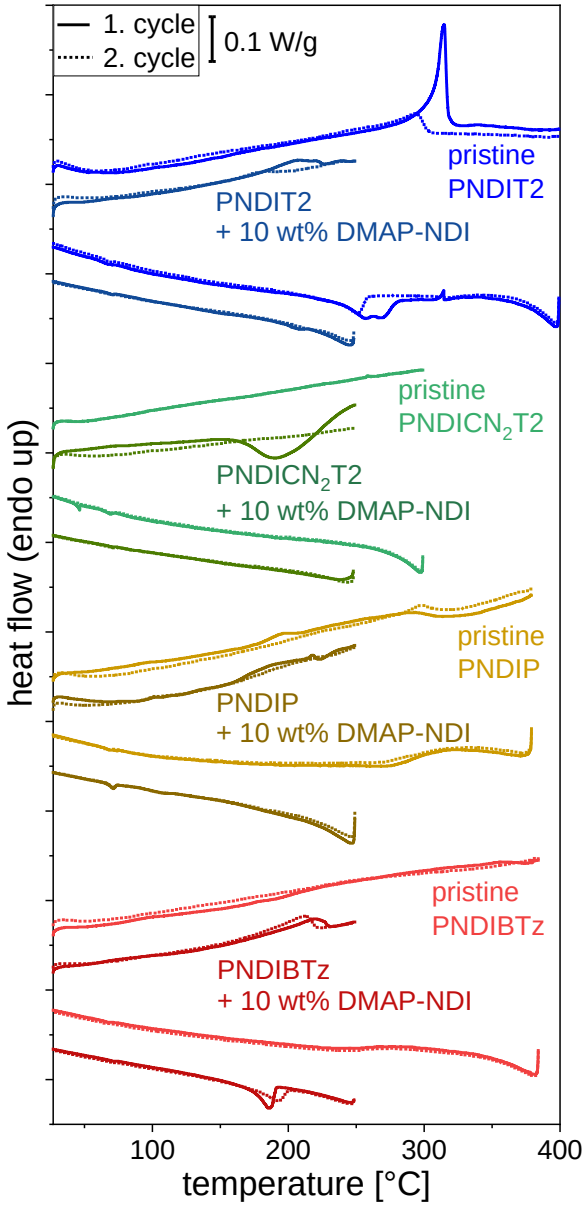

Figure 7. DSC measurements of pristine NDI copolymers and solution blends with 10 wt% DMAP-NDI. Heating and cooling rates 10 $K \cdot min^{-1}$, endo up, under N_2.

To further evaluate the aspect of miscibility of DMAP-NDI and the copolymers, grazing incidence wide angle X-ray scattering (GIWAXS) was performed on both pristine and doped films. Figure **8** compares the 2D scattering

patterns of pristine and doped films, while Figures S11-S15 in the SI also present 1D line profiles. Comparison of the neat samples reveals differences in the degree of microstructural order. PNDIT2 exhibits the highest degree of order, with the 2D scattering profile of this polymer exhibiting well-defined lamellar stacking, backbone stacking and π-π stacking peaks consistent with earlier results.[62] Indeed, multiple orders of lamellar stacking and backbone reflections are seen pointing to a high degree or order. All the other polymers exhibit a reduced degree of microstructural order compared to PNDIT2. PNDICN_2T2 in particular appears to be nearly amorphous, with only a weak lamellar stacking peak at 2.5 nm^{-1} observable (note that the sharp peaks at ~ 15.5 nm^{-1} are from silicon dust from cleaving of the substrate). The other polymers show clearer lamellar stacking peaks than PNDICN_2T2 but do not match the degree of order shown by PNDIT2. Based on the sharpness of the lamellar stacking peak and number of peaks present, the neat polymer films can be ranked in terms of degree of microstructural order as PNDIT2 > PNDIP > PNDIBTz > PNDICN_2T2. With doping, the crystalline peaks from the polymer remain essentially unchanged, but with the appearance of new peaks associated with the crystalline phase of the dopant molecule DMAP-NDI.[15] In particular, a prominent peak located at ~ 4.5 nm^{-1} along the Q_z (out-of-plane) is visible along with a number of other peaks located off-axis, characteristic of a highly ordered crystalline phase of the small molecule dopant. Interestingly, there are strong differences in the degree of scattering seen from the crystalline phase of DMAP-NDI that appears to be correlated with the degree of crystalline order of the polymer. In particular, for PNDICN_2T2 showing very weak crystalline order in the neat film, there is also very weak scattering from the dopant molecule in the PNDICN_2T2 / DMAP-NDI blend. These observations can be understood in terms of a relatively good miscibility between the dopant and the relatively amorphous PNDICN_2T2. In contrast, for the more crystalline polymers, such as PNDIT2, PNDIP and PNDIBTz, strong scattering from the dopant can be seen in the doped films, indicating a poor miscibility between dopant and polymer. These results agree well with those from DSC, where DMAP-NDI melting is found for PNDIT2, PNDIP and PNDIBTz.

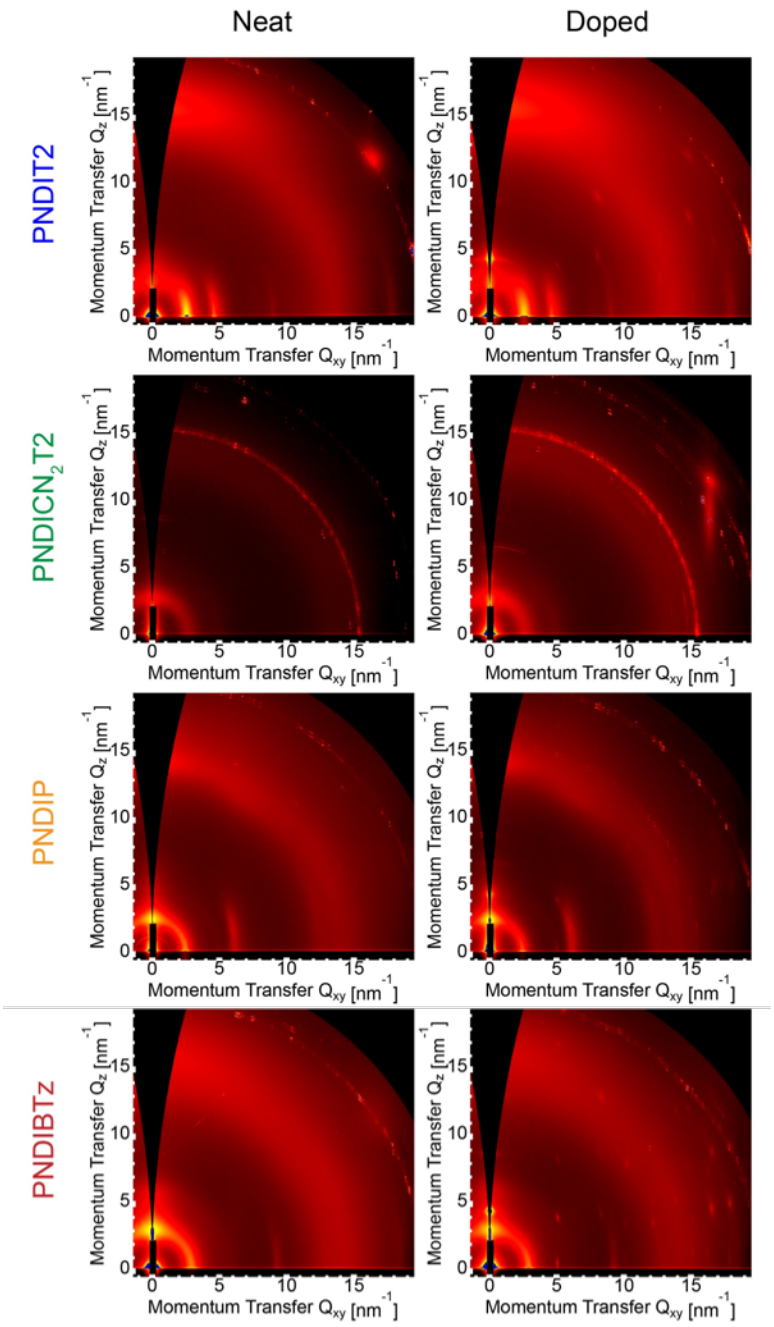

Figure 8. Two-dimensional GIWAXS scattering patterns of pristine and doped (10 wt% DMAP-NDI) NDI-copolymer films.

The electrical properties of NDI copolymer/ DMAP-NDI blends were also investigated. The electrical resistances of thin film NDI copolymers samples doped with 10 and 20 wt% DMAP-NDI were measured and the corresponding conductivities were calculated and listed in Table S3. Figure 9 gives a graphical representation of the data for better illustration.

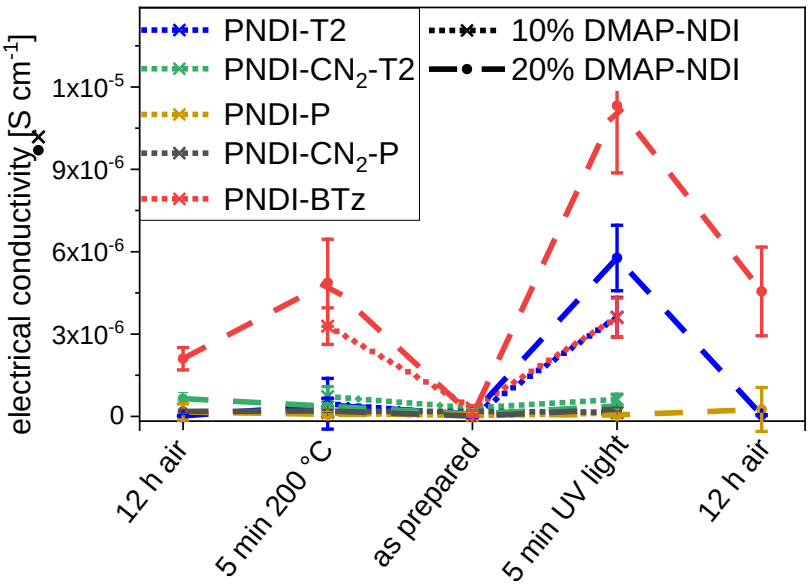

Figure 9. Electrical conductivities of NDI copolymer films doped with a) 10 wt% and b) 20 wt% DMAP-NDI.

Doped with 10 wt% DMAP-NDI, PNDIT2 and PNDIBTz showed the highest electrical conductivities despite their significantly lower radical anion concentrations. After UV activation, their resistance decreases by up to two orders of magnitude, although the resulting conductivity of $3.6 \cdot 10^{-6}$ S·cm^{-1} still lags behind typical values for PNDIT2 doped with *N*-DMBI or tetrakis(dimethylamino)ethylene (TDAE) (reported around 10^{-3} S·cm^{-1}).[27,34,36] Increasing the DMAP-NDI content to 20 wt% increases conductivities of PNDIT2 and PNDIBTz to $5.8 \cdot 10^{-6}$ and $1.1 \cdot 10^{-5}$ S·cm^{-1}, respectively. Thermal activation gave rise to lower conductivities in both cases, which is in line with the lower radical anion yields seen with EPR measurements. The opposite is true for the cyanated NDI copolymers: despite high radical anion yields, the measured electrical conductivity values are low. Since the measured currents were close to the detection limit of the device, a large uncertainty factor in the conductivity values has to be expected, and a discussion about the exact values must be omitted. While, after one day of air exposure, PNDIT2 reported very low values of electrical conductivity (around 10^{-8} S cm^{-1}) and PNDIBTz reduced the electrical conductivity value to about $4.6 \cdot 10^{-6}$ S·cm^{-1}, the conductivities of the cyanated polymers remain stable. This trend is also confirmed by the EPR and UV-Vis measurements, in which PNDICN$_2$T2 and PNDICN$_2$P showed practically the same radical anion concentration after one day of air exposure. This further corroborates

the key role of the LUMO energy level to achieve processability and operation of n-type devices under ambient conditions.

One factor rationalizing the low conductivities of the NDI copolymers doped with DMAP-NDI compared to N-benzimidazole-based dopants may be Coulomb attraction between localized radical anions and nitrogen-based radical cations of the DMAP-NDI side chain, which may limit conductivity.[63] The low conductivities of the two cyanated NDI copolymers, which display both high radical anion yields and air stability, can be further understood on the basis of increased backbone torsion, yielding localized electron densities and low electron mobilities. With their large amount of charge carriers n probed by ESR spectroscopy, the corresponding low electrical conductivities σ have to be the results of low electron mobilities μ ($\sigma = \mu \cdot e \cdot n$). Indeed, as an example, bottom contact, top-gate field-effect transistors (FETs) of $PNDICN_2T2$, which are similar to devices used for the investigation of PNDIT2[51] and PNDIBTz[52], gave low electron mobilities < 10^{-5} $cm^2 \cdot V^{-1}s^{-1}$. This is approximately five orders of magnitude lower than for PNDIT2 and three orders of magnitude lower than for PNDIBTz. Thus, the larger number of charge carriers found for the cyanated NDI copolymers does not compensate the severe limits of electron transport, which explains the herein seen low electrical conductivities.

3. Conclusions

In this work, we studied the influence of HOMO and LUMO energy levels of five different NDI copolymers on the thermally and photochemically induced doping with a small molecule NDI having a dimethylaminopropyl (DMAP) side chains. Both the NDI core (NDI and dicyanated NDI, $NDICN_2$) as well as the donor comonomer (phenylene P, bithiophene T2, bithiazole BTz) were structurally varied. EPR measurements showed markedly higher radical anion yields for the cyanated NDI copolymers which are characterized by much lower LUMO energy levels. Almost two orders of magnitude higher radical anion concentrations were found in thermally activated $PNDICN_2T2$ and a 40 times higher radical anion concentration in $PNDICN_2P$ compared to their non-cyanated analogs. Photochemically induced doping enabled a higher doping yield for $PNDICN_2P$ than for $PNDICN_2T2$ as a result of the lower HOMO of the former. All cyanated NDI copolymers also showed excellent air stability of their radical anions. Next to electronic factors, a further aspect enabling high doping efficacy may

be an increased miscibility of the cyanated NDI copolymers with DMAP-NDI, which in turn is the result of reduced crystallinity. Despite their highest radical anion concentrations, electrical conductivities of the cyanated NDI copolymers were moderate, which can be rationalized by a significant backbone torsion, localization of the radical anions and the resulting low electron mobility. Nevertheless, air stability of radical anions was confirmed by stable electrical conductivity under ambient conditions. In summary, this work provides general guidelines for designing electron acceptor polymers suitable to give air stable radical anions as well as high conductivities.

ASSOCIATED CONTENT

Supporting Information. Instruments and methods, syntheses, NMR, SEC, UV-Vis, EPR, thermal and GIWAXS characterizations are available free of charge (PDF).

AUTHOR INFORMATION

Corresponding Author

*e-mail: Michael.Sommer@chemie.tu-chemnitz.de

Present Addresses

†Physikalische Chemie und Didaktik der Chemie, Universität des Saarlandes, Campus B2 2, 66123 Saarbrücken, Germany

Author Contributions

The manuscript was written through contributions of all authors. All authors have given approval to the final version of the manuscript.

Funding Sources

S. S. thanks the Deutsche Bundesstiftung Umwelt for financial support. M. C. and A. P. acknowledge of the European Research Council (ERC) under the European Union's Horizon 2020 research and innovation

programme “HEROIC”, grant agreement 638059. D.F. acknowledges the Deutsche Forschungsgemeinschaft (DFG) for the grant “Molecular Understanding of Thermo-Electric Properties in Organic Polymers” (FA 1502/1-1), and the Regional Computing Centre (RRZK) of Universität zu Köln, for providing computing time and resources on the HPC CHEOPS.

ACKNOWLEDGMENT

The authors acknowledge Desiree Adamczak for SEC measurements and Fritz Nübling for providing NDI precursors. This work was performed in part on the SAXS/WAXS beamline[64] at the Australian Synchrotron, part of ANSTO.

ABBREVIATIONS

CT	charge transfer
CV	cyclic voltammetry
cw-EPR	continuous wave electron paramagnetic resonance
DAP	direct arylation polycondensation
DFT	density functional theory
DMAP	dimethylaminopropyl
DSC	differential scanning colometry
E_{opt}, exp and E_{opt}, theo	optical band gaps from UV-Vis / CV and DFT calculations, respectively
FET	field- effect transistors
GIWAXS	grazing-incidence wide-angle X-ray scattering
HOMO	highest occupied molecular orbital
LUMO	lowest unoccupied molecular orbital
M_n / M_w	number / weight average molecular weight
N-DBI	dihydro-1H-benzimidazole-2-yl
NDI	naphthalene diimide
PET	photoinduced electron transfer
PNDI-BTz	poly{(NDI-2,6-diyl)-*alt*-5,5‘-(2,2‘-bithiazole)}
PNDI-CN_2-P	poly{(NDI-3,7-dicyano-2,6-diyl)-*alt*-1,4-phenylene}
PNDI-CN_2-T2	poly{(NDI-3,7-dicyano-2,6-diyl)-*alt*-5,5‘-(2,2‘-bithiophen)}
PNDI-P	poly{(NDI-2,6-diyl)-*alt*-1,4-phenylene}
PNDI-T2	poly{(NDI-2,6-diyl)-*alt*-5,5‘-(2,2‘-bithiophen)}
redox	reduction-oxidation
SEC	size exclusion chromatography
SP	Stille polycondensation
SPC	Suzuki polycondensation
TDAE	Tetrakis(dimethylamino)ethylene
T_m	melting temperature

REFERENCES

(1) Anthony, J. E.; Facchetti, A.; Heeney, M.; Marder, S. R.; Zhan, X. N-Type Organic Semiconductors in Organic Electronics. *Adv. Mater.* **2010**, *22* (34), 3876–3892. https://doi.org/10.1002/adma.200903628.

(2) Würthner, F.; Stolte, M. Naphthalene and Perylene Diimides for Organic Transistors. *Chem. Commun.* **2011**, *47* (18), 5109–5115. https://doi.org/10.1039/C1CC10321K.

(3) Kroon, R.; Mengistie, D. A.; Kiefer, D.; Hynynen, J.; Ryan, J. D.; Yu, L.; Müller, C. Thermoelectric Plastics: From Design to Synthesis, Processing and Structure–Property Relationships. *Chem. Soc. Rev.* **2016**, *45* (22), 6147–6164. https://doi.org/10.1039/C6CS00149A.

(4) Shi, K.; Zhang, F.; Di, C.-A.; Yan, T.-W.; Zou, Y.; Zhou, X.; Zhu, D.; Wang, J.-Y.; Pei, J. Toward High Performance N-Type Thermoelectric Materials by Rational Modification of BDPPV Backbones. *J. Am. Chem. Soc.* **2015**, *137* (22), 6979–6982. https://doi.org/10.1021/jacs.5b00945.

(5) Zhou, H.; Yang, L.; Price, S. C.; Knight, K. J.; You, W. Enhanced Photovoltaic Performance of Low-Bandgap Polymers with Deep LUMO Levels. *Angew. Chem.* **2010**, *122* (43), 8164–8167. https://doi.org/10.1002/ange.201003357.

(6) Facchetti, A.; Yoon, M.-H.; Stern, C. L.; Katz, H. E.; Marks, T. J. Building Blocks for N-Type Organic Electronics: Regiochemically Modulated Inversion of Majority Carrier Sign in Perfluoroarene-Modified Polythiophene Semiconductors. *Angew. Chem. Int. Ed.* **2003**, *42* (33), 3900–3903. https://doi.org/10.1002/anie.200351253.

(7) Tang, S.; Li, W.; Shen, F.; Liu, D.; Yang, B.; Ma, Y. Highly Efficient Deep-Blue Electroluminescence Based on the Triphenylamine-Cored and Peripheral Blue Emitters with Segregative HOMO–LUMO Characteristics. *J. Mater. Chem.* **2012**, *22* (10), 4401–4408. https://doi.org/10.1039/C1JM14639D.

(8) Rossbauer, S.; Müller, C.; Anthopoulos, T. D. Comparative Study of the N-Type Doping Efficiency in Solution-Processed Fullerenes and Fullerene Derivatives. *Adv. Funct. Mater.* **2014**, *24* (45), 7116–7124. https://doi.org/10.1002/adfm.201401842.

(9) Qi, Y.; Mohapatra, S. K.; Bok Kim, S.; Barlow, S.; Marder, S. R.; Kahn, A. Solution Doping of Organic Semiconductors Using Air-Stable n-Dopants. *Appl. Phys. Lett.* **2012**, *100* (8), 083305. https://doi.org/10.1063/1.3689760.

(10) Walzer, K.; Maennig, B.; Pfeiffer, M.; Leo, K. Highly Efficient Organic Devices Based on Electrically Doped Transport Layers. *Chem. Rev.* **2007**, *107* (4), 1233–1271. https://doi.org/10.1021/cr050156n.

(11) Yan, K.; Li, C.-Z. Solution-Processable Conductive Organics via Anion-Induced n-Doping and Their Applications in Organic and Perovskite Solar Cells. *Macromol. Chem. Phys.* **2019**, *220* (10), 1900084. https://doi.org/10.1002/macp.201900084.

(12) Chueh, C.-C.; Li, C.-Z.; Ding, F.; Li, Z.; Cernetic, N.; Li, X.; Jen, A. K.-Y. Doping Versatile N-Type Organic Semiconductors via Room Temperature Solution-Processable Anionic Dopants. *ACS Appl. Mater. Interfaces* **2017**, *9* (1), 1136–1144. https://doi.org/10.1021/acsami.6b14375.

(13) Jones, B. A.; Ahrens, M. J.; Yoon, M.-H.; Facchetti, A.; Marks, T. J.; Wasielewski, M. R. High-Mobility Air-Stable n-Type Semiconductors with Processing Versatility: Dicyanoperylene-3,4:9,10-Bis(Dicarboximides). *Angew. Chem. Int. Ed.* **2004**, *43* (46), 6363–6366. https://doi.org/10.1002/anie.200461324.

(14) Jones, B. A.; Facchetti, A.; Wasielewski, M. R.; Marks, T. J. Tuning Orbital Energetics in Arylene Diimide Semiconductors. Materials Design for Ambient Stability of n-Type Charge Transport. *J. Am. Chem. Soc.* **2007**, *129* (49), 15259–15278. https://doi.org/10.1021/ja075242e.

(15) Schmidt, S.; Biskup, T.; Jiao, X.; R. McNeill, C.; Sommer, M. Controlling Intermolecular Redox-Doping of Naphthalene Diimides. *J. Mater. Chem. C* **2019**, *7* (15), 4466–4474. https://doi.org/10.1039/C9TC00721K.

(16) Zhao, X.; Madan, D.; Cheng, Y.; Zhou, J.; Li, H.; Thon, S. M.; Bragg, A. E.; DeCoster, M. E.; Hopkins, P. E.; Katz, H. E. High Conductivity and Electron-Transfer Validation in an n-Type Fluoride-Anion-Doped Polymer for Thermoelectrics in Air. *Adv. Mater.* **2017**, *29* (34), 1606928. https://doi.org/10.1002/adma.201606928.

(17) Thalacker, C.; Röger, C.; Würthner, F. Synthesis and Optical and Redox Properties of Core-Substituted Naphthalene Diimide Dyes. *J. Org. Chem.* **2006**, *71* (21), 8098–8105. https://doi.org/10.1021/jo0612269.

(18) Miros, F. N.; Matile, S. Core-Substituted Naphthalenediimides: LUMO Levels Revisited, in Comparison with Preylenediimides with Sulfur Redox Switches in the Core. *ChemistryOpen* **2016**, *5* (3), 219–226. https://doi.org/10.1002/open.201500222.
(19) Suraru, S.-L.; Würthner, F. Strategies for the Synthesis of Functional Naphthalene Diimides. *Angew. Chem. Int. Ed.* **2014**, *53* (29), 7428–7448. https://doi.org/10.1002/anie.201309746.
(20) Chen, D.; Avestro, A.-J.; Chen, Z.; Sun, J.; Wang, S.; Xiao, M.; Erno, Z.; Algaradah, M. M.; Nassar, M. S.; Amine, K.; Meng, Y.; Stoddart, J. F. A Rigid Naphthalenediimide Triangle for Organic Rechargeable Lithium-Ion Batteries. *Adv. Mater.* **2015**, *27* (18), 2907–2912. https://doi.org/10.1002/adma.201405416.
(21) Al Kobaisi, M.; Bhosale, S. V.; Latham, K.; Raynor, A. M.; Bhosale, S. V. Functional Naphthalene Diimides: Synthesis, Properties, and Applications. *Chem. Rev.* **2016**, *116* (19), 11685–11796. https://doi.org/10.1021/acs.chemrev.6b00160.
(22) Schneebeli, S. T.; Frasconi, M.; Liu, Z.; Wu, Y.; Gardner, D. M.; Strutt, N. L.; Cheng, C.; Carmieli, R.; Wasielewski, M. R.; Stoddart, J. F. Electron Sharing and Anion–π Recognition in Molecular Triangular Prisms. *Angew. Chem.* **2013**, *125* (49), 13338–13342. https://doi.org/10.1002/ange.201307984.
(23) Schroot, R.; Schlotthauer, T.; Schubert, U. S.; Jäger, M. Modular Assembly of Poly(Naphthalene Diimide) and Ru(II) Dyes for an Efficient Light-Induced Charge Separation in Hierarchically Controlled Polymer Architectures. *Macromolecules* **2016**, *49* (6), 2112–2123. https://doi.org/10.1021/acs.macromol.5b02717.
(24) Sommer, M. Conjugated Polymers Based on Naphthalene Diimide for Organic Electronics. *J. Mater. Chem. C* **2014**, *2* (17), 3088–3098. https://doi.org/10.1039/C3TC31755B.
(25) Guo, X.; Facchetti, A.; Marks, T. J. Imide- and Amide-Functionalized Polymer Semiconductors. *Chem. Rev.* **2014**, *114* (18), 8943–9021. https://doi.org/10.1021/cr500225d.
(26) Saglio, B.; Mura, M.; Massetti, M.; Scuratti, F.; Beretta, D.; Jiao, X.; McNeill, C. R.; Sommer, M.; Famulari, A.; Lanzani, G.; Caironi, M.; Bertarelli, C. N-Alkyl Substituted 1H-Benzimidazoles as Improved n-Type Dopants for a Naphthalene-Diimide Based Copolymer. *J. Mater. Chem. A* **2018**, *6* (31), 15294–15302. https://doi.org/10.1039/C8TA04901G.
(27) Wang, S.; Sun, H.; Ail, U.; Vagin, M.; Persson, P. O. Å.; Andreasen, J. W.; Thiel, W.; Berggren, M.; Crispin, X.; Fazzi, D.; Fabiano, S. Thermoelectric Properties of Solution-Processed n-Doped Ladder-Type Conducting Polymers. *Adv. Mater.* **2016**, *28* (48), 10764–10771. https://doi.org/10.1002/adma.201603731.
(28) Fabiano, S.; Braun, S.; Liu, X.; Weverberghs, E.; Gerbaux, P.; Fahlman, M.; Berggren, M.; Crispin, X. Poly(Ethylene Imine) Impurities Induce n-Doping Reaction in Organic (Semi)Conductors. *Adv. Mater.* **2014**, *26* (34), 6000–6006. https://doi.org/10.1002/adma.201401986.
(29) Guha, S.; Goodson, F. S.; Corson, L. J.; Saha, S. Boundaries of Anion/Naphthalenediimide Interactions: From Anion−π Interactions to Anion-Induced Charge-Transfer and Electron-Transfer Phenomena. *J. Am. Chem. Soc.* **2012**, *134* (33), 13679–13691. https://doi.org/10.1021/ja303173n.
(30) Zheng, X.; Zhang, Y.; Cao, N.; Li, X.; Zhang, S.; Du, R.; Wang, H.; Ye, Z.; Wang, Y.; Cao, F.; Li, H.; Hong, X.; Sue, A. C.-H.; Yang, C.; Liu, W.-G.; Li, H. Coulombic-Enhanced Hetero Radical Pairing Interactions. *Nat. Commun.* **2018**, *9* (1), 1–9. https://doi.org/10.1038/s41467-018-04335-0.
(31) Guo, S.; Kim, S. B.; Mohapatra, S. K.; Qi, Y.; Sajoto, T.; Kahn, A.; Marder, S. R.; Barlow, S. N-Doping of Organic Electronic Materials Using Air-Stable Organometallics. *Adv. Mater.* **2012**, *24* (5), 699–703. https://doi.org/10.1002/adma.201103238.
(32) Schlitz, R. A.; Brunetti, F. G.; Glaudell, A. M.; Miller, P. L.; Brady, M. A.; Takacs, C. J.; Hawker, C. J.; Chabinyc, M. L. Solubility-Limited Extrinsic n-Type Doping of a High Electron Mobility Polymer for Thermoelectric Applications. *Adv. Mater.* **2014**, *26* (18), 2825–2830. https://doi.org/10.1002/adma.201304866.
(33) *Physics of Organic Semiconductors*, 2nd completely new rev. ed.; Brütting, W., Adachi, C., Holmes, R. J. D., Eds.; Wiley-VCH: Weinheim, Germany, 2012; Vol. 3.
(34) Shin, Y.; Massetti, M.; Komber, H.; Biskup, T.; Nava, D.; Lanzani, G.; Caironi, M.; Sommer, M. Improving Miscibility of a Naphthalene Diimide-Bithiophene Copolymer with n-Type Dopants through the Incorporation of "Kinked" Monomers. *Adv. Electron. Mater.* **2018**, *4* (10), 1700581. https://doi.org/10.1002/aelm.201700581.
(35) Kiefer, D.; Giovannitti, A.; Sun, H.; Biskup, T.; Hofmann, A.; Koopmans, M.; Cendra, C.; Weber, S.; Anton Koster, L. J.; Olsson, E.; Rivnay, J.; Fabiano, S.; McCulloch, I.; Müller, C. Enhanced N-Doping Efficiency

of a Naphthalenediimide-Based Copolymer through Polar Side Chains for Organic Thermoelectrics. *ACS Energy Lett.* **2018**, *3* (2), 278–285. https://doi.org/10.1021/acsenergylett.7b01146.
(36) Gregg, B. A.; Chen, S.-G.; Branz, H. M. On the Superlinear Increase in Conductivity with Dopant Concentration in Excitonic Semiconductors. *Appl. Phys. Lett.* **2004**, *84* (10), 1707–1709. https://doi.org/10.1063/1.1668326.
(37) Gregg, B. A.; Cormier, R. A. Doping Molecular Semiconductors: N-Type Doping of a Liquid Crystal Perylene Diimide. *J. Am. Chem. Soc.* **2001**, *123* (32), 7959–7960. https://doi.org/10.1021/ja016410k.
(38) Reilly, T. H.; Hains, A. W.; Chen, H.-Y.; Gregg, B. A. A Self-Doping, O2-Stable, n-Type Interfacial Layer for Organic Electronics. *Adv. Energy Mater.* **2012**, *2* (4), 455–460. https://doi.org/10.1002/aenm.201100446.
(39) Russ, B.; Robb, M. J.; Brunetti, F. G.; Miller, P. L.; Perry, E. E.; Patel, S. N.; Ho, V.; Chang, W. B.; Urban, J. J.; Chabinyc, M. L.; Hawker, C. J.; Segalman, R. A. Power Factor Enhancement in Solution-Processed Organic n-Type Thermoelectrics Through Molecular Design. *Adv. Mater.* **2014**, *26* (21), 3473–3477. https://doi.org/10.1002/adma.201306116.
(40) Russ, B.; Robb, M. J.; Popere, B. C.; Perry, E. E.; Mai, C.-K.; Fronk, S. L.; Patel, S. N.; Mates, T. E.; Bazan, G. C.; Urban, J. J.; Chabinyc, M. L.; Hawker, C. J.; Segalman, R. A. Tethered Tertiary Amines as Solid-State n-Type Dopants for Solution-Processable Organic Semiconductors. *Chem. Sci.* **2016**, *7* (3), 1914–1919. https://doi.org/10.1039/C5SC04217H.
(41) Liu, Y.; Page, Z. A.; Russell, T. P.; Emrick, T. Finely Tuned Polymer Interlayers Enhance Solar Cell Efficiency. *Angew. Chem. Int. Ed.* **2015**, *54* (39), 11485–11489. https://doi.org/10.1002/anie.201503933.
(42) Matsunaga, Y.; Goto, K.; Kubono, K.; Sako, K.; Shinmyozu, T. Photoinduced Color Change and Photomechanical Effect of Naphthalene Diimides Bearing Alkylamine Moieties in the Solid State. *Chem. Eur. J.* **2014**, *20* (24), 7309–7316. https://doi.org/10.1002/chem.201304849.
(43) Saha, S. Anion-Induced Electron Transfer. *Acc. Chem. Res.* **2018**, *51* (9), 2225–2236. https://doi.org/10.1021/acs.accounts.8b00197.
(44) Ajayakumar, M. R.; Mukhopadhyay, P. Naphthalene-Bis-Hydrazimide: Radical Anions and ICT as New Bimodal Probes for Differential Sensing of a Library of Amines. *Chem. Commun.* **2009**, No. 25, 3702–3704. https://doi.org/10.1039/B903097B.
(45) Jia, T.; Sun, C.; Xu, R.; Chen, Z.; Yin, Q.; Jin, Y.; Yip, H.-L.; Huang, F.; Cao, Y. Naphthalene Diimide Based N-Type Conjugated Polymers as Efficient Cathode Interfacial Materials for Polymer and Perovskite Solar Cells. *ACS Appl. Mater. Interfaces* **2017**, *9* (41), 36070–36081. https://doi.org/10.1021/acsami.7b10365.
(46) Wang, Z.; Zheng, N.; Zhang, W.; Yan, H.; Xie, Z.; Ma, Y.; Huang, F.; Cao, Y. Self-Doped, n-Type Perylene Diimide Derivatives as Electron Transporting Layers for High-Efficiency Polymer Solar Cells. *Adv. Energy Mater.* **2017**, *7* (15), 1700232. https://doi.org/10.1002/aenm.201700232.
(47) Guo, X.; Kim, F. S.; Seger, M. J.; Jenekhe, S. A.; Watson, M. D. Naphthalene Diimide-Based Polymer Semiconductors: Synthesis, Structure–Property Correlations, and n-Channel and Ambipolar Field-Effect Transistors. *Chem. Mater.* **2012**, *24* (8), 1434–1442. https://doi.org/10.1021/cm2034273.
(48) Chen, H.; Liu, Z.; Zhao, Z.; Zheng, L.; Tan, S.; Yin, Z.; Zhu, C.; Liu, Y. Synthesis, Structural Characterization, and Field-Effect Transistor Properties of n-Channel Semiconducting Polymers Containing Five-Membered Heterocyclic Acceptors: Superiority of Thiadiazole Compared with Oxadiazole. *ACS Appl. Mater. Interfaces* **2016**, *8* (48), 33051–33059. https://doi.org/10.1021/acsami.6b12540.
(49) Yang, L.; Xiao, C.; Jiang, W.; Wang, Z. Conjugated Donor-Acceptor Copolymers from Dicyanated Naphthalene Diimide. *Tetrahedron* **2014**, *70* (36), 6265–6270. https://doi.org/10.1016/j.tet.2014.04.002.
(50) Chang, J.; Ye, Q.; Huang, K.-W.; Zhang, J.; Chen, Z.-K.; Wu, J.; Chi, C. Stepwise Cyanation of Naphthalene Diimide for N-Channel Field-Effect Transistors. *Org. Lett.* **2012**, *14* (12), 2964–2967. https://doi.org/10.1021/ol300914k.
(51) Matsidik, R.; Komber, H.; Luzio, A.; Caironi, M.; Sommer, M. Defect-Free Naphthalene Diimide Bithiophene Copolymers with Controlled Molar Mass and High Performance via Direct Arylation Polycondensation. *J. Am. Chem. Soc.* **2015**, *137* (20). https://doi.org/10.1021/jacs.5b03355.
(52) Matsidik, R.; Giorgio, M.; Luzio, A.; Caironi, M.; Komber, H.; Sommer, M. A Defect-Free Naphthalene Diimide Bithiazole Copolymer via Regioselective Direct Arylation Polycondensation. *Eur. J. Org. Chem.* **2018**, *2018* (44), 6121–6126. https://doi.org/10.1002/ejoc.201800821.

(53) Kim, Y.; Hong, J.; Oh, J. H.; Yang, C. Naphthalene Diimide Incorporated Thiophene-Free Copolymers with Acene and Heteroacene Units: Comparison of Geometric Features and Electron-Donating Strength of Co-Units. *Chem. Mater.* **2013**, *25* (15), 3251–3259. https://doi.org/10.1021/cm401829x.
(54) Dreuw, A.; Head-Gordon, M. Single-Reference Ab Initio Methods for the Calculation of Excited States of Large Molecules. *Chem. Rev.* **2005**, *105* (11), 4009–4037. https://doi.org/10.1021/cr0505627.
(55) Frisch, M. J.; Trucks, G. W.; Schlegel, H. B.; Scuseria, G. E.; Robb, M. A.; Cheeseman, J. R.; Scalmani, G.; Barone, V.; Petersson, G. A.; Nakatsuji, H.; Li, X.; Caricato, M.; Marenich, A. V.; Bloino, J.; Janesko, B. G.; Gomperts, R.; Mennucci, B.; Hratchian, H. P.; Ortiz, J. V.; Izmaylov, A. F.; Sonnenberg, J. L.; Williams-Young, D.; Ding, F.; Lipparini, F.; Egidi, F.; Goings, J.; Peng, B.; Petrone, A.; Henderson, T.; Ranasinghe, D.; Zakrzewski, V. G.; Gao, J.; Rega, N.; Zheng, G.; Liang, W.; Hada, M.; Ehara, M.; Toyota, K.; Fukuda, R.; Hasegawa, J.; Ishida, M.; Nakajima, T.; Honda, Y.; Kitao, O.; Nakai, H.; Vreven, T.; Throssell, K.; Montgomery, J. A., Jr.; Peralta, J. E.; Ogliaro, F.; Bearpark, M. J.; Heyd, J. J.; Brothers, E. N.; Kudin, K. N.; Staroverov, V. N.; Keith, T. A.; Kobayashi, R.; Normand, J.; Raghavachari, K.; Rendell, A. P.; Burant, J. C.; Iyengar, S. S.; Tomasi, J.; Cossi, M.; Millam, J. M.; Klene, M.; Adamo, C.; Cammi, R.; Ochterski, J. W.; Martin, R. L.; Morokuma, K.; Farkas, O.; Foresman, J. B.; Fox, D. J. *Gaussian 16 Rev. C.01*; Wallingford, CT, 2016.
(56) Klauk, H. *Organic Electronics II: More Materials and Applications*; John Wiley & Sons, 2012.
(57) Matsidik, R.; Luzio, A.; Askin, Ö.; Fazzi, D.; Sepe, A.; Steiner, U.; Komber, H.; Caironi, M.; Sommer, M. Highly Planarized Naphthalene Diimide–Bifuran Copolymers with Unexpected Charge Transport Performance. *Chem. Mater.* **2017**, *29* (13), 5473–5483. https://doi.org/10.1021/acs.chemmater.6b05313.
(58) Matsidik, R.; Martin, J.; Schmidt, S.; Obermayer, J.; Lombeck, F.; Nübling, F.; Komber, H.; Fazzi, D.; Sommer, M. C–H Arylation of Unsubstituted Furan and Thiophene with Acceptor Bromides: Access to Donor–Acceptor–Donor-Type Building Blocks for Organic Electronics. *J. Org. Chem.* **2015**, *80* (2), 980–987. https://doi.org/10.1021/jo502432e.
(59) Umeyama, T.; Takamatsu, T.; Tezuka, N.; Matano, Y.; Araki, Y.; Wada, T.; Yoshikawa, O.; Sagawa, T.; Yoshikawa, S.; Imahori, H. Synthesis and Photophysical and Photovoltaic Properties of Porphyrin−Furan and −Thiophene Alternating Copolymers. *J. Phys. Chem. C* **2009**, *113* (24), 10798–10806. https://doi.org/10.1021/jp902001z.
(60) Gosztola, D.; Niemczyk, M. P.; Svec, W.; Lukas, A. S.; Wasielewski, M. R. Excited Doublet States of Electrochemically Generated Aromatic Imide and Diimide Radical Anions. *J. Phys. Chem. A* **2000**, *104* (28), 6545–6551. https://doi.org/10.1021/jp000706f.
(61) V. Bhosale, S.; H. Jani, C.; J. Langford, S. Chemistry of Naphthalene Diimides. *Chem. Soc. Rev.* **2008**, *37* (2), 331–342. https://doi.org/10.1039/B615857A.
(62) Rivnay, J.; Toney, M. F.; Zheng, Y.; Kauvar, I. V.; Chen, Z.; Wagner, V.; Facchetti, A.; Salleo, A. Unconventional Face-On Texture and Exceptional In-Plane Order of a High Mobility n-Type Polymer. *Adv. Mater.* **2010**, *22* (39), 4359–4363. https://doi.org/10.1002/adma.201001202.
(63) Mityashin, A.; Olivier, Y.; Regemorter, T. V.; Rolin, C.; Verlaak, S.; Martinelli, N. G.; Beljonne, D.; Cornil, J.; Genoe, J.; Heremans, P. Unraveling the Mechanism of Molecular Doping in Organic Semiconductors. *Adv. Mater.* **2012**, *24* (12), 1535–1539. https://doi.org/10.1002/adma.201104269.
(64) Kirby, N. M.; Mudie, S. T.; Hawley, A. M.; Cookson, D. J.; Mertens, H. D. T.; Cowieson, N.; Samardzic-Boban, V. A Low-Background-Intensity Focusing Small-Angle X-Ray Scattering Undulator Beamline. *J. Appl. Cryst.* **2013**, *46* (6), 1670–1680. https://doi.org/10.1107/S002188981302774X.